Supplementary Material

Phosphorization engineering ameliorated electrocatalytic activity for overall water splitting on Ni$_3$S$_2$ nanosheets

Pengyan Wang, [a] Honglin He, [b] Zonghua Pu, [a] Lei Chen, [a]** Chengtian Zhang, [a] Zhe Wang, [a] and Shichun Mu[a]*

[a] State Key Laboratory of Advanced Technology for Materials Synthesis and Processing, Wuhan University of Technology, Wuhan 430070, China

[b] Central Theater Command General Hospital of the Chinese People's Liberation Army, Wuhan 430070, China

* Corresponding author

** Corresponding author

E-mail: msc@whut.edu.cn (S. Mu), chl0588@163.com (L. Chen).

1. Experimental Section

1.1. Chemicals.

$Ni(NO_3)_2 \cdot 6H_2O$, thiourea, KOH, hexamethylene tetramine (HMT) and $NaH_2PO_2 \cdot H_2O$ were obtained from Aladdin Reagent Ltd. Acetone and absolute ethanol were acquired from Beijing Chemical Works Ltd. Nafion (5 wt %), Pt/C (20 wt %) and IrO_2 were provided by Sigma-Aldrich. All the reagents in the experiments were analytical grade and used as received. High purity water supplied by the Millipore system was used as a solvent.

1.2. Preparation of Ni₂P/NF.

The Ni_2P/NF was synthesized through a hydrothermal route following by phosphorization. First, the NF was immersed into a 35 mL homogeneous solution containing 10 mmol HMT and 5 mmol $Ni(NO_3)_2 \cdot 6H_2O$. Next, the solution with NF was transferred into a 50 mL Teflon-lined stainless steel autoclave and treated at 100 °C for 10 h to obtain Ni precursor on NF. To obtain Ni_2P/NF, the Ni precursor and $NaH_2PO_2 \cdot H_2O$ (the molar ratio of metal ion to phosphorus was 1 to 5) were put at the center and upstream side of the tube furnace, respectively. The sample was then annealed at 300 °C for 2 h under continuous N_2 atmosphere. Subsequently, the tube furnace was cooled down naturally and obtained the black product Ni_2P/NF.

1.3. Preparation of Ni₃S₂/NF.

At first, a piece of Ni foam (NF) (2 cm × 3 cm) was carefully sonicated in acetone, absolute ethanol and deionized water for 5 min to remove the surface oxides. Afterwards, the weight of the pretreated NF was weighed and recorded. After that, the Ni_3S_2/NF electrode was prepared via a typical hydrothermal procedure: 6 mmol $Ni(NO_3)_2 \cdot 6H_2O$ and 4 mmol thiourea were dissolved in deionized water by stirring about 30 min. Next, the cleaned NF was transferred into a 50 mL Teflon-lined stainless steel autoclave containing the above homogeneous

solution and treated at 120 °C for 6 h. After the system naturally cooled down to room temperature, the Ni_3S_2/NF was washed with ethanol and deionized water several times and then dried at 60 °C for 12 h under vacuum.

1.4. Preparation of Ni_3S_2-Ni_2P/NF.

The Ni_2P-Ni_3S_2/NF was prepared by a partial phosphorization reaction between Ni_3S_2/NF and $NaH_2PO_2 \cdot H_2O$. Briefly, the Ni_3S_2/NF and 2 g of $NaH_2PO_2 \cdot H_2O$ were placed at the centre and upstream of a tube furnace. After flushed with high purity N_2, the furnace was heated to 270 °C and maintained at this temperature for 30 min. Continuous N_2 flow was maintained throughout the heating process and the subsequent natural cooling. For comparative studies, two additional samples were prepared under the same synthetic procedures expect that the quality of $NaH_2PO_2 \cdot H_2O$ was changed to 1 g and 4 g. The mass loading of electrocatalysts on NF was about 6 mg cm^{-2}.

1.5. Material Characterization.

The morphology and structure were characterized by the field emission scanning electron microscopy (FE-SEM Zeiss Ultra Plus) and transmission electron microscopy (TEM JEM2100F). Power X-ray diffraction (XRD) patterns were collected on a Bruker D8 Advance. Inductively Coupled Plasma-Optical Emission Spectr (ICP-OES) analysis was performed on Prodigy 7. X-ray photoelectron spectroscopy (XPS) measurements were carried out on an ESCALABMK II X-ray photoelectron spectrometer.

1.6. Electrochemical Measurements.

All electrochemical measurements were performed on a CHI 660E electrochemical workstation (CHI Instruments, Shanghai, China) in a standard three-electrode system. The as-prepared catalysts on NF were directly utilized as working electrode. A Hg/HgO and graphite rod were used as the reference and the counter electrodes, respectively. The dispersed IrO_2 or

Pt/C ink was obtained by ultrasonication of the mixture of 6 mg of IrO_2 or Pt/C, 500 μL of ethanol, 500 μL of water and 50 μL of 5 wt % Nafion. Then, the catalyst ink was coated on NF (loading: 6 mg cm^{-2}). All linear sweep voltammetry (LSV) curves were conducted in 1 M KOH at 25 °C with a scan rate of 5 mV s^{-1} unless specifcally stated. In HER and OER measurements, the Hg/HgO reference electrode was calibrated with respect to RHE by adding a value of 0.924 V. The obtained polarization curves for HER and OER were iR-corrected，where R is the solution resistance (2.2 Ω in 1 M KOH). Electrochemical impedance spectroscopy (EIS) analysis was carried out in the frequency range of 0.1 Hz to 100 kHz. The double layer capacitance (C_{dl}) was determined by cyclic voltammetry (CV) curves at various scan rates of 20, 40, 60, 80, 100, 120, and 140 mV s^{-1} in -0.51 ~ -0.57 V versus Hg/HgO region.
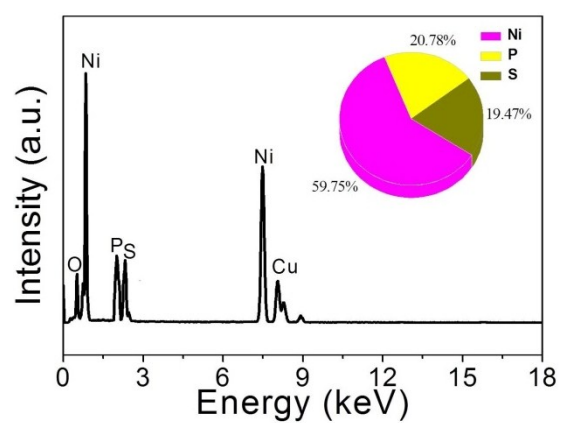
Figure S1. EDX spectrum of Ni$_3$S$_2$-Ni$_2$P/NF (inset: pie pattern of element distribution)
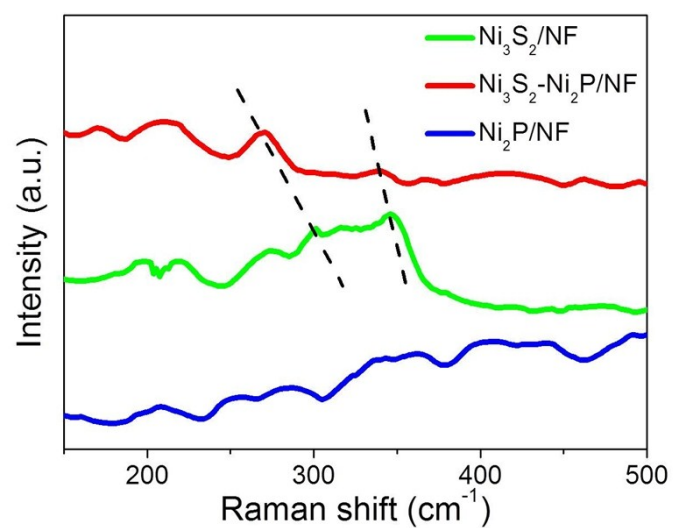
Figure S2. Raman spectra of Ni_2P/NF, Ni_3S_2/NF and Ni_3S_2-Ni_2P/NF.
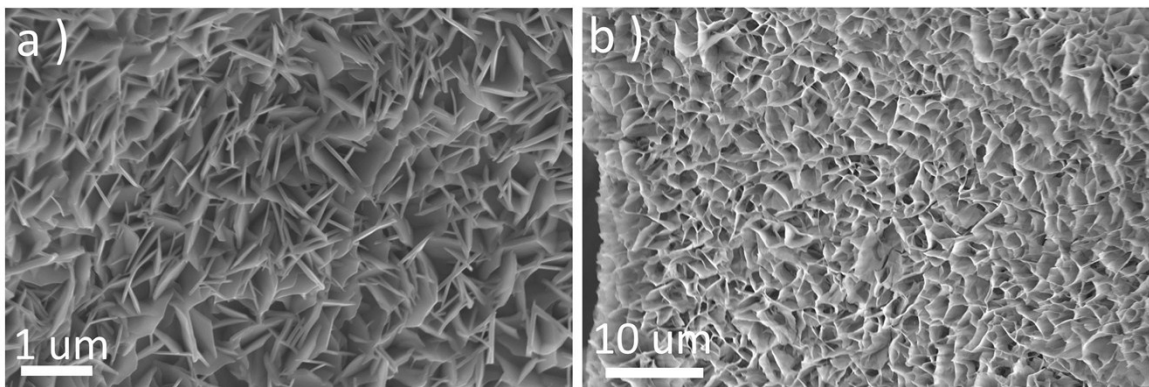
Figure S3. (a) SEM image of Ni_3S_2/NF. (b) SEM image of Ni_2P/NF.
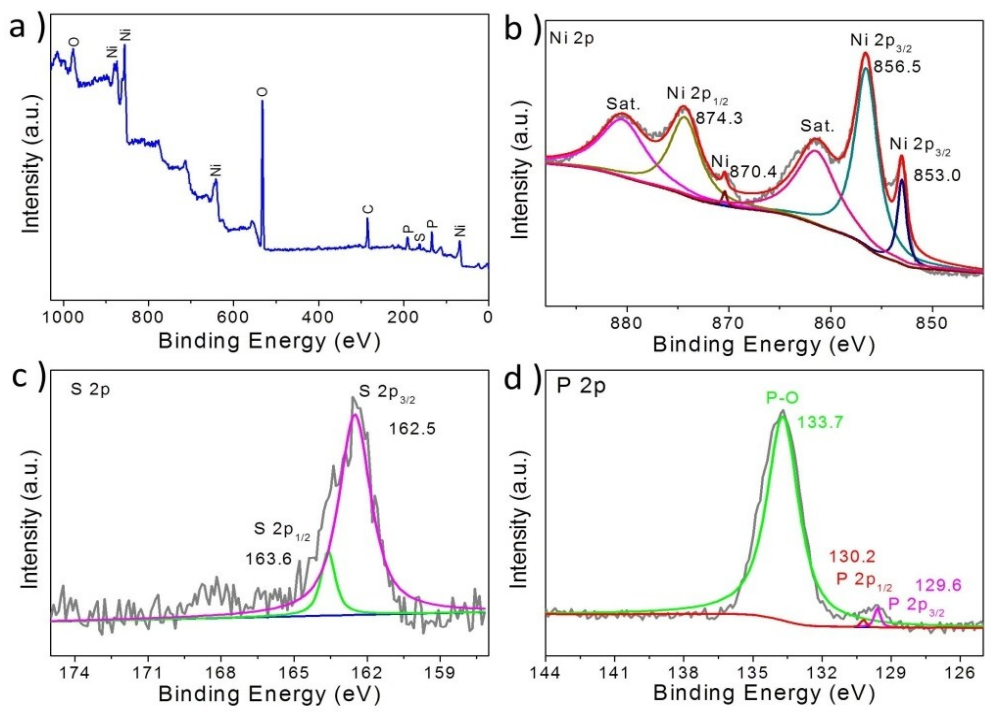
Figure S4. (a) XPS survey spectrum for Ni_3S_2-Ni_2P/NF. Core level (b) Ni 2p, (c) S 2p and (d)

P 2p XPS spectra collected for Ni_3S_2-Ni_2P/NF.
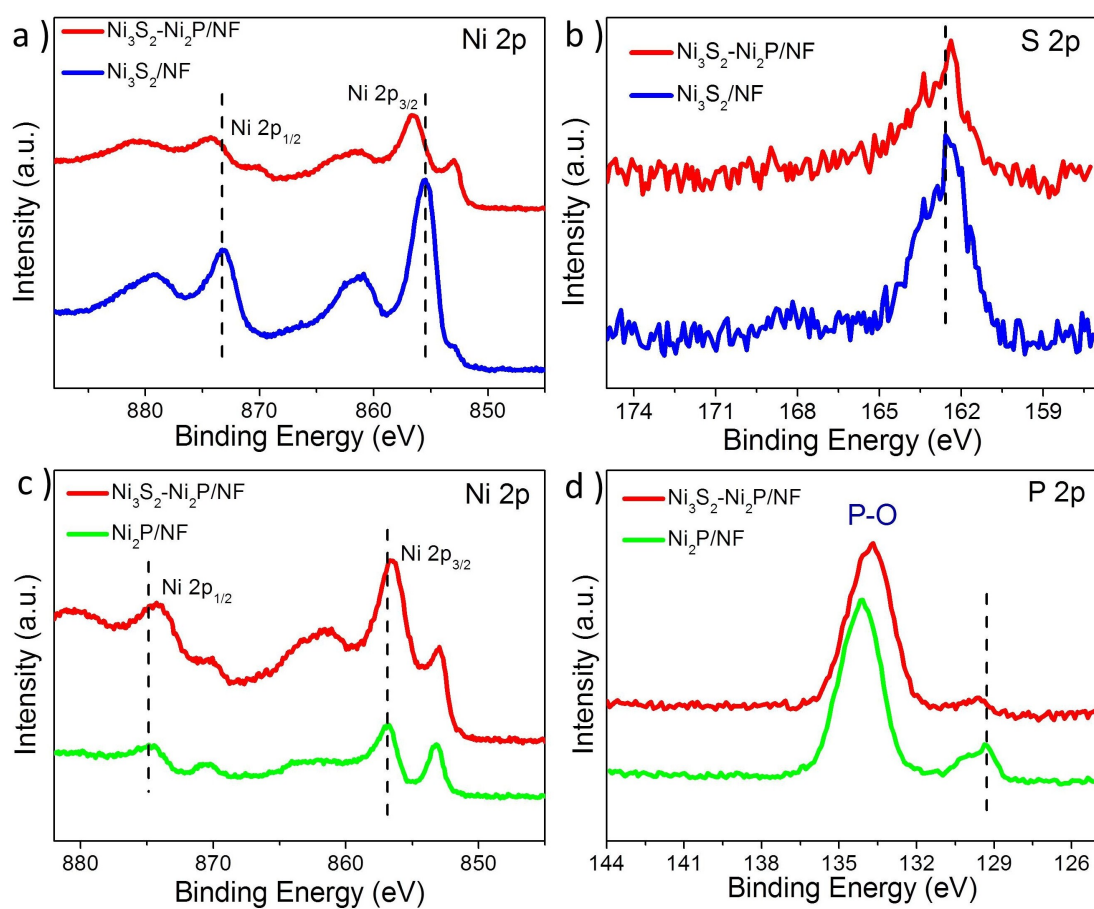
Figure S5. (a) Ni 2p and (b) S 2p XPS spectra of Ni_3S_2/NF and Ni_3S_2-Ni_2P/NF. (c) Ni 2p and (d) P 2p XPS spectra of Ni_2P/NF and Ni_3S_2-Ni_2P/NF.
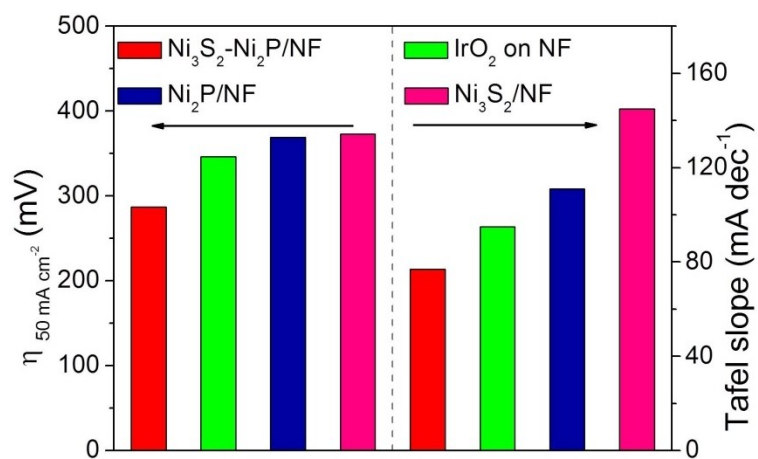
Figure S6. Overpotentials at j = 50 mA cm^{-2} (left) and Tafel slopes (right) for IrO$_2$ on NF, Ni$_2$P/NF, Ni$_3$S$_2$/NF and Ni$_3$S$_2$-Ni$_2$P/NF in 1 M KOH
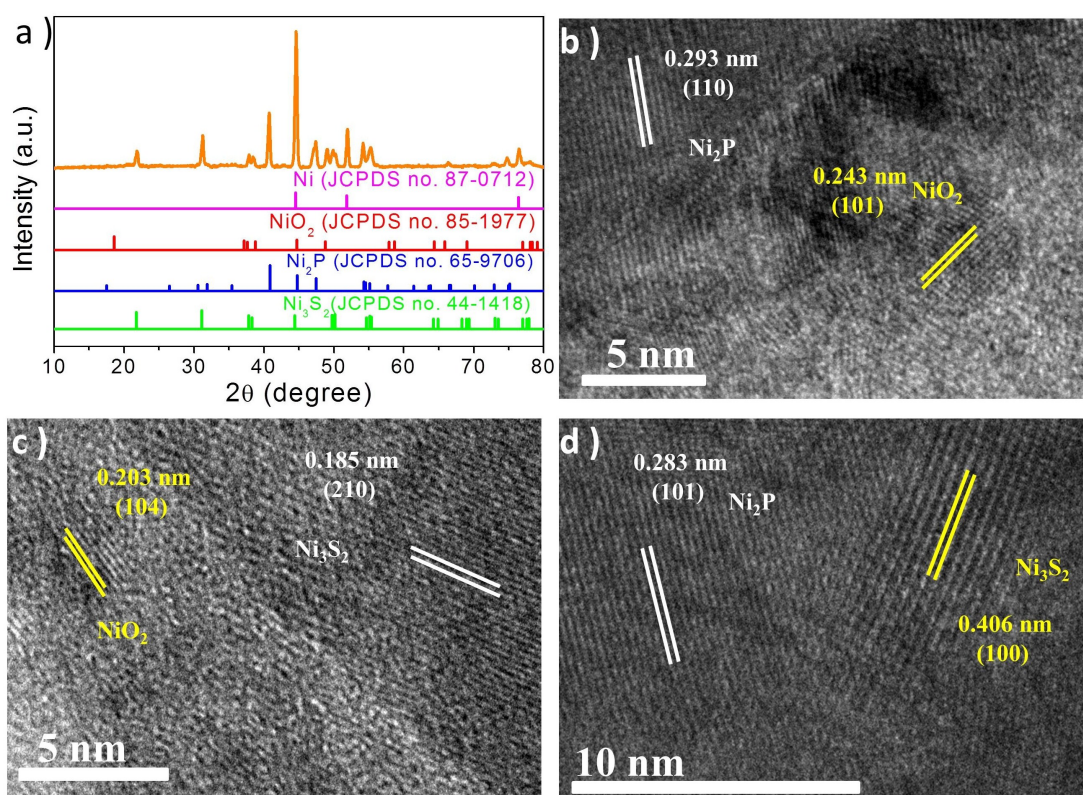
Figure S7. (a) XRD pattern and (b-d) HRTEM images of Ni_3S_2-Ni_2P/NF after OER test.
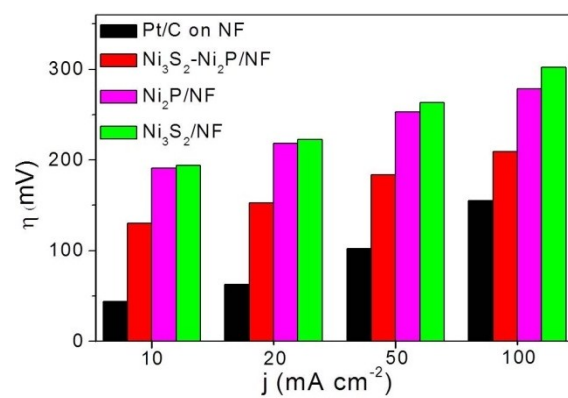
Figure S8. Overpotentials at at j= 10, 20, 50 and 100 mA cm^{-2} of Pt/C on NF, Ni$_2$P/NF,

Ni$_3$S$_2$/NF and Ni$_3$S$_2$-Ni$_2$P/NF.
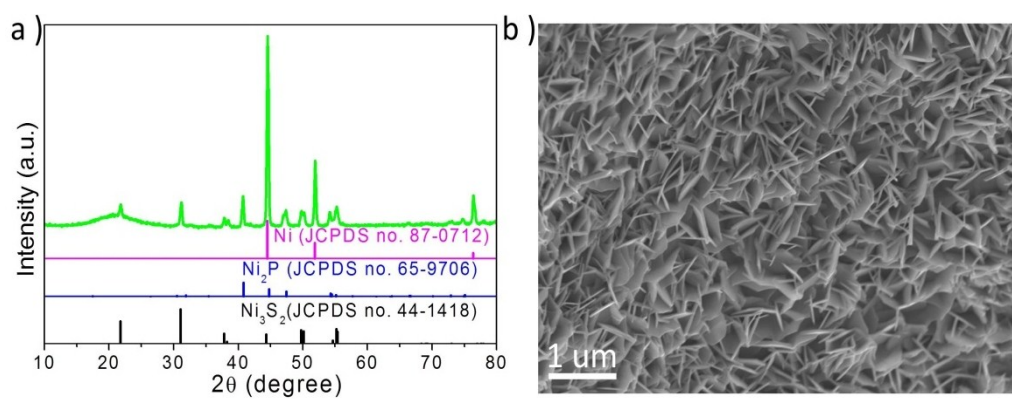
Figure S9. XRD pattern (a) and SEM image (b) of Ni_3S_2-Ni_2P/NF after long-term HER stability test.
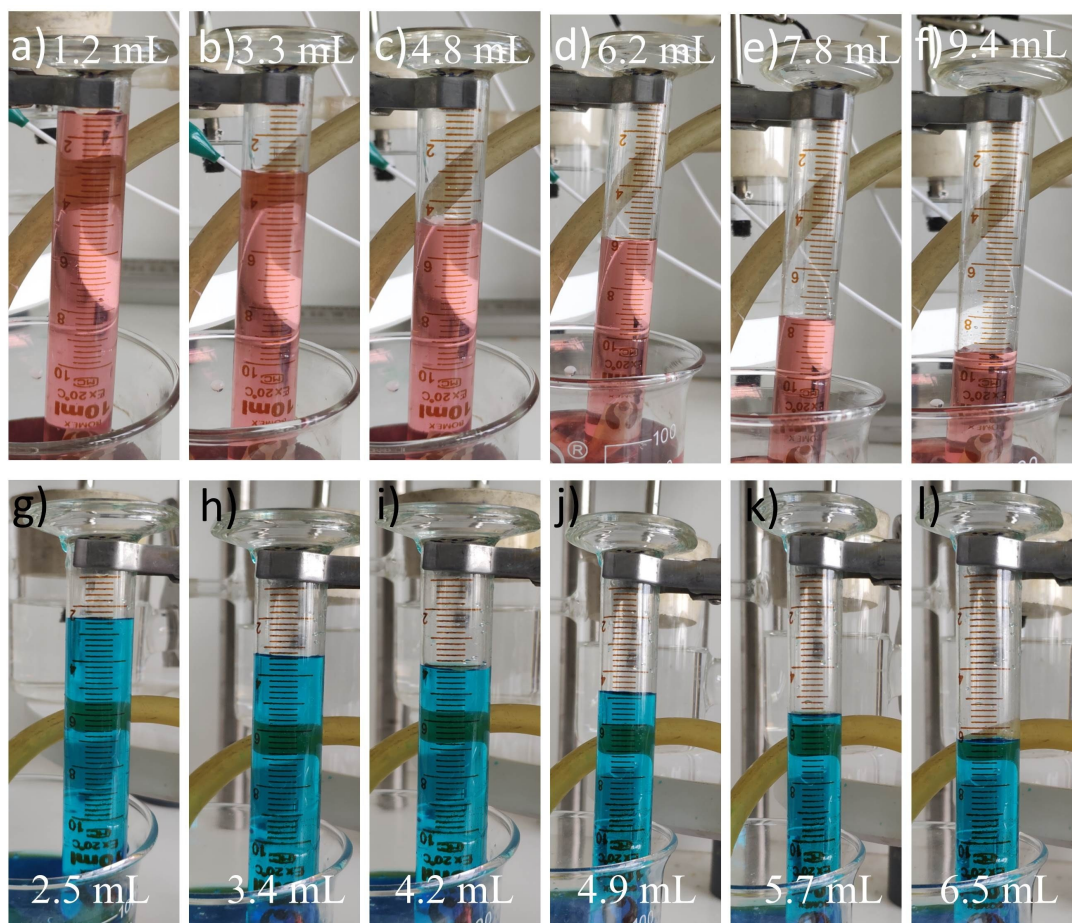
Figure S10. (a, b, c, d, e, f) Corresponding levels of hydrogen gas generated at 0s, 200s, 400s, 600s, 800s, 1000s. (g, h, i, j, k, l) Corresponding levels of oxygen gas generated at 0s, 200s, 400s, 600s, 800s, 1000s.
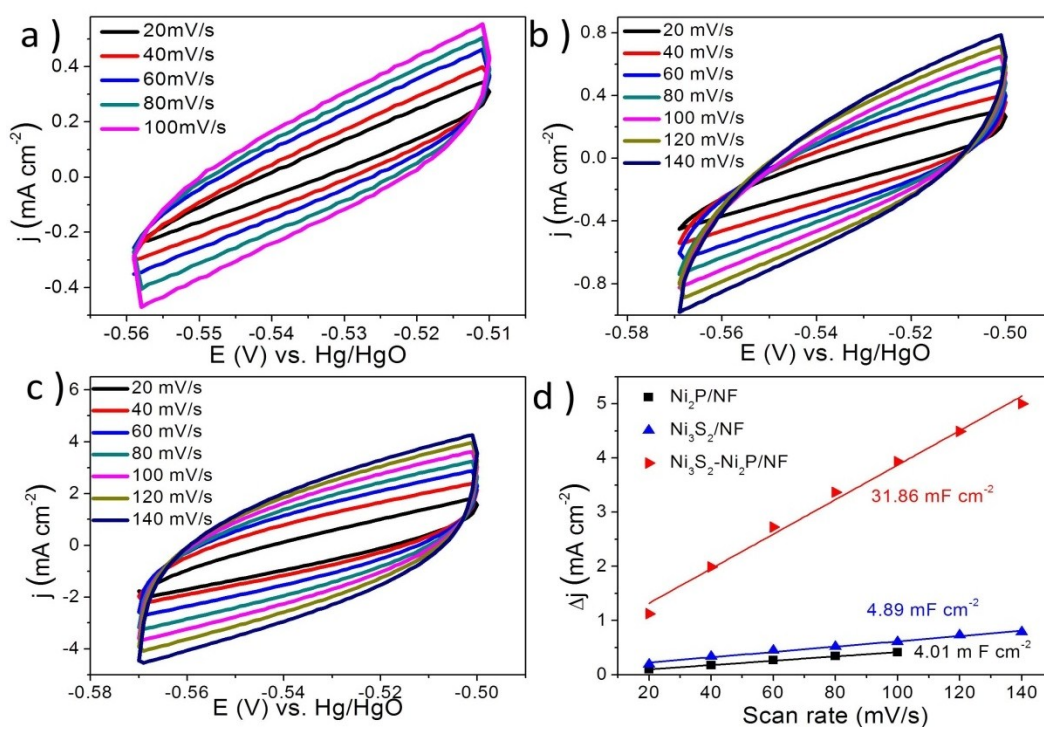
Figure S11. Cyclic voltammogram (CV) curves at different scan rates for (a) Ni_2P/NF, (b) Ni_3S_2/NF and (c) $Ni_3S_2-Ni_2P/NF$. The current density variation at 0.535 V versus Hg/HgO plotted against with the scan rates (d).
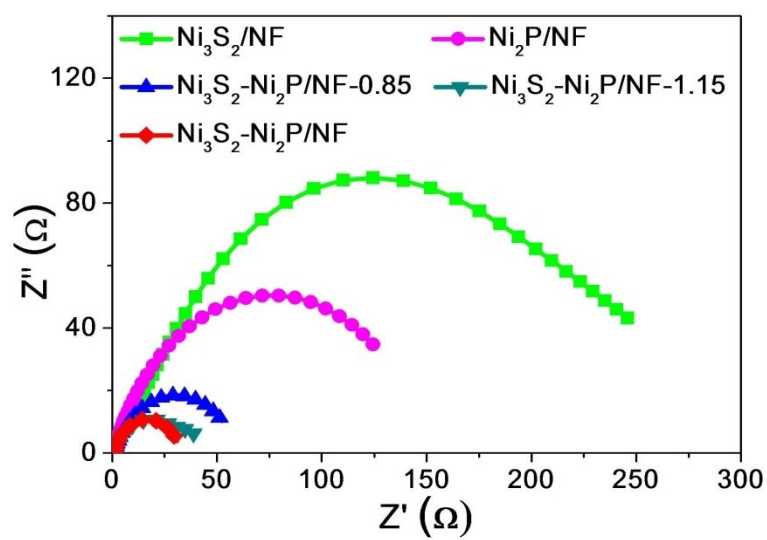
Figure S12. Nyquist plots of Ni_2P/NF, Ni_3S_2/NF, Ni_3S_2-Ni_2P/NF, Ni_3S_2-Ni_2P/NF-1.15 and

Ni_3S_2-Ni_2P/NF-0.85 recorded in 1 M KOH.
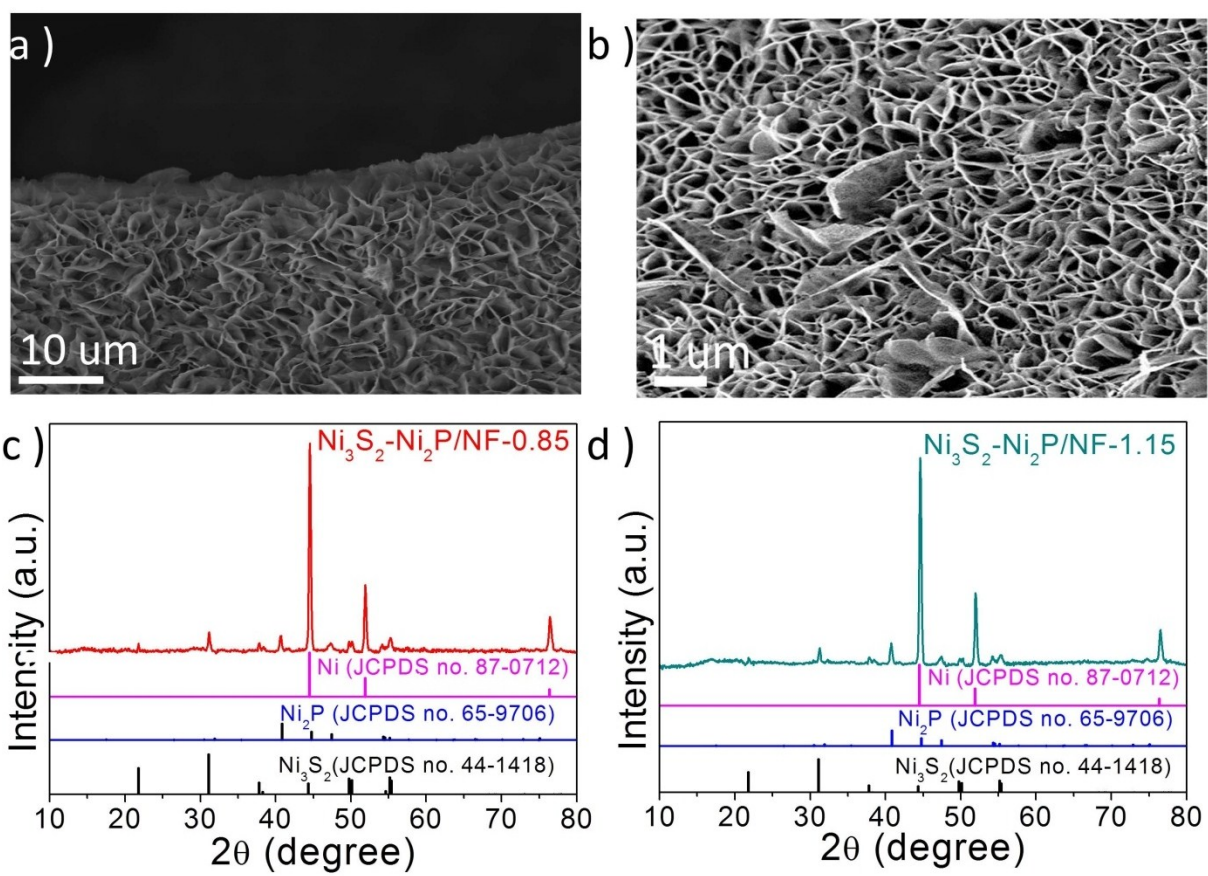
Figure S13. (a) SEM image and (c) XRD pattern of Ni$_3$S$_2$-Ni$_2$P/NF-0.85. (b) SEM image and

(d) XRD pattern of Ni$_3$S$_2$-Ni$_2$P/NF-1.15.
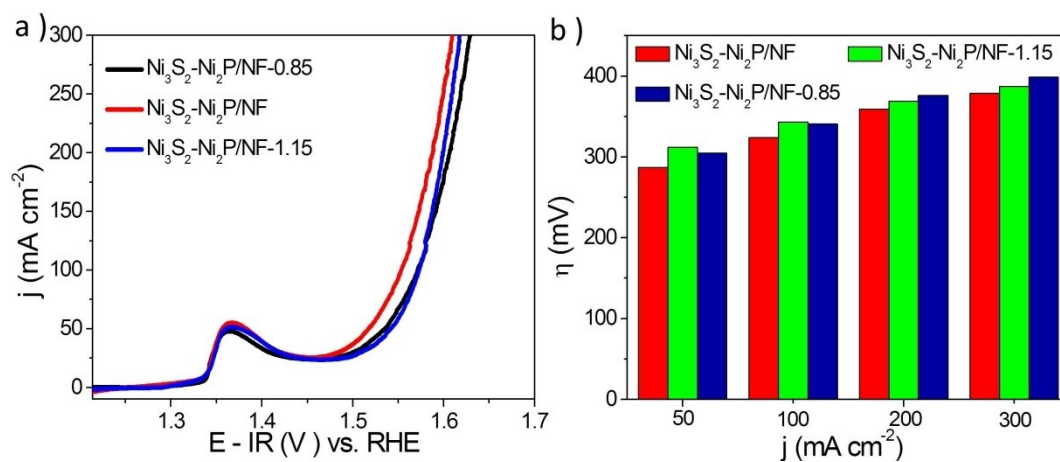
Figure S14. (a) Polarization curves and (b) overpotentials at j= 50, 100, 200 and 300 mA cm^{-2} of a series of Ni$_3$S$_2$-Ni$_2$P/NF with different P/S molar ratios for OER in 1 M KOH.
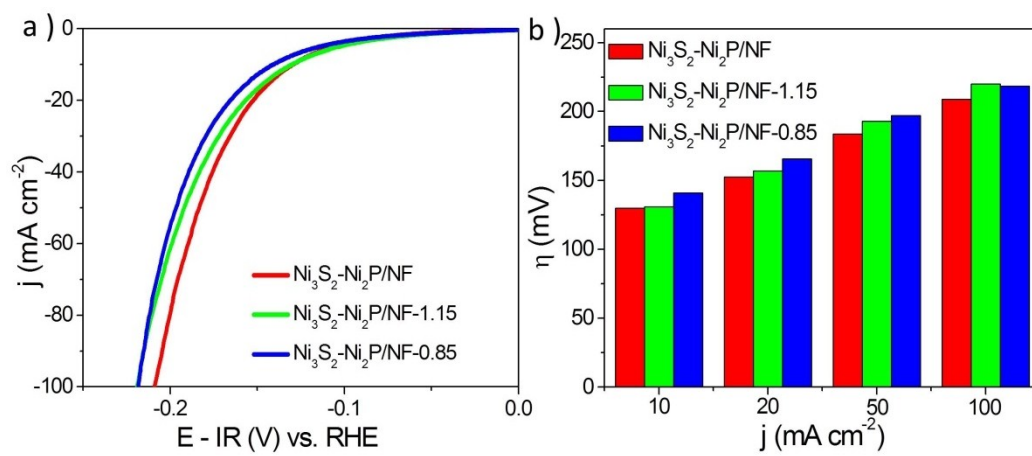
Figure S15. (a) Polarization curves and (b) overpotentials at j= 10, 20, 50 and 100 mA cm^{-2}

of a series of Ni$_3$S$_2$-Ni$_2$P/NF with different P/S molar ratios in 1 M KOH.
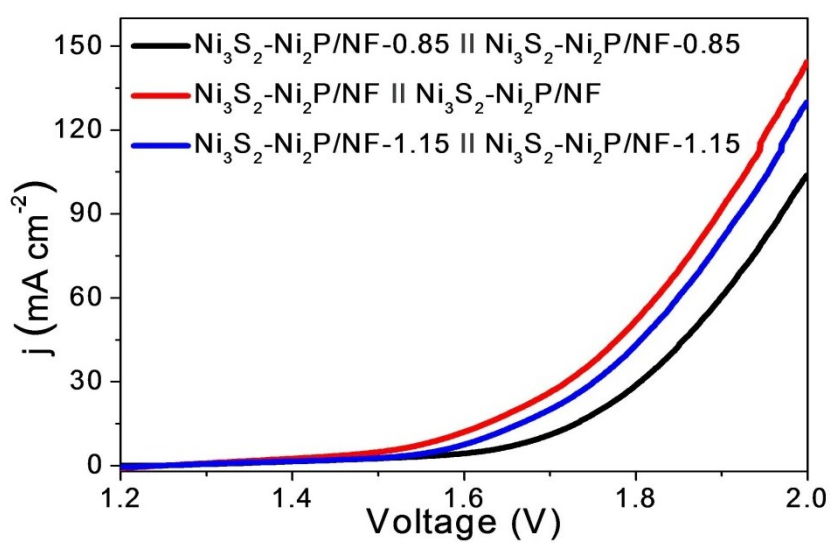
Figure S16. Polarization curves of a series of Ni_3S_2-Ni_2P/NF||Ni_3S_2-Ni_2P/NF electrolytic cells with different P/S molar ratios toward overall water splitting in 1 M KOH at a scan rate of 5 mV s^{-1}.
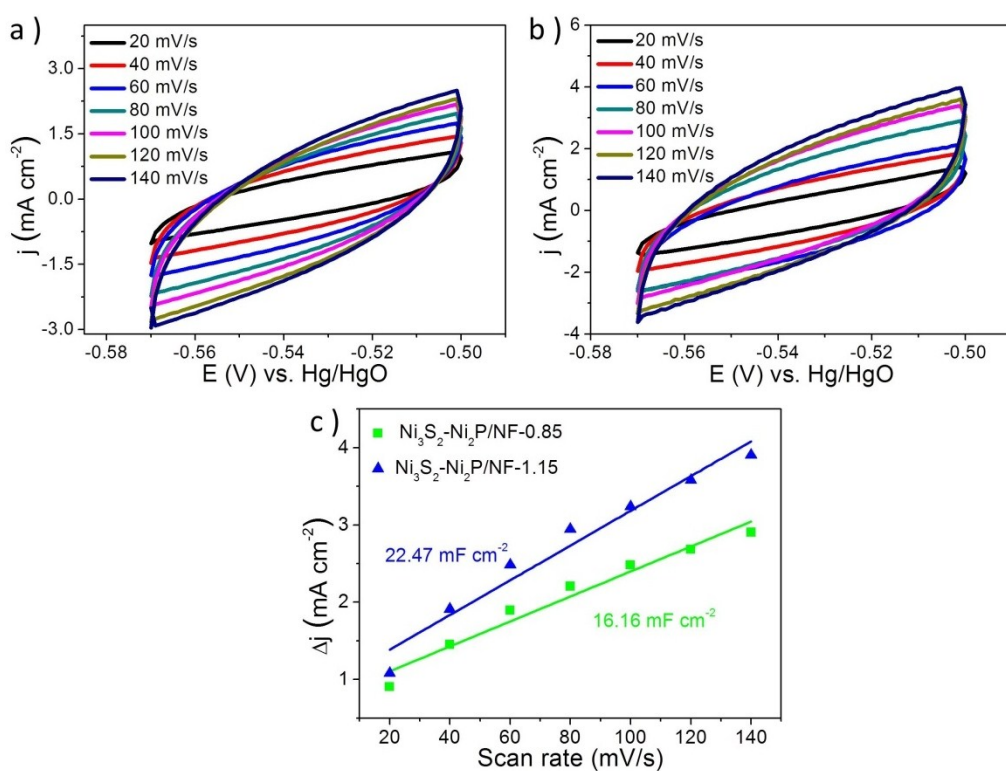
Figure S17. Cyclic voltammogram (CV) curves at different scan rates for (a) Ni_3S_2-Ni_2P/NF-0.85 and (b) Ni_3S_2-Ni_2P/NF-1.15. (c) The current density variation at 0.535 V versus Hg/HgO plotted against with the scan rates.

Table S1. ICP-OES analysis data for the molar ratios of P and S elements in the as-prepared

Ni_2P-Ni_3S_2/NF catalysts.

Sample	Ni_3S_2-Ni_2P/NF-0.85	Ni_3S_2-Ni_2P/NF	Ni_3S_2-Ni_2P/NF-1.15
Quality of $NaH_2PO_2 \cdot H_2O$ (g)	1g	2g	4g
Mass percentage of S (%)	14.63	12.91	12.69
Mass percentage of P (%)	11.97	13.29	14.11
Molar ratio of P/S	0.85	1.07	1.15

Table S2. Comparison of OER performance for Ni_3S_2-Ni_2P/NF with other reported OER electrocatalysts.

Catalysts	Overpotential@j (mV@mA cm^{-2})	Electrolytes	Ref.
Ni_3S_2-Ni_2P/NF	287@50	1 M KOH	This work
$Ni_{0.75}V_{0.25}$-LDH	350@10	1M KOH	1
NiO_x/NiOOH	320@10	1 M NaOH	2
NiFe LDHs	305@10	1 M KOH	3
$Ni_{45}Fe_{55}$ oxyhydroxide	310@10	0.1 M KOH	4
CoCr LDH	340@10	1 M NaOH	5
NiO	347@20	1 M KOH	6
Ni_3N/NF	399@20	1 M KOH	7
Ni_2P nanoparticles	290@10	1M KOH	8
Co_4N/CC	257@10	1 M KOH	9
Ni-Co-P HNBs	270@10	1 M KOH	10
$Na_{0.08}Ni_{0.9}Fe_{0.1}O_2$	260@10	1 M KOH	11
MoS_2-Ni_3S_2 HNRs/NF	249@10	1 M KOH	12
3D-Co/ cobaltphytate nanoplates	265@10	1 M KOH	13
FeNi-rGO LDH	206@10	1 M KOH	14

Table S3. Comparison of HER performance in 1 M KOH for Ni_3S_2-Ni_2P/NF with other reported HER electrocatalysts.

Catalysts	Overpotential (mV) at 10 mA cm^{-2}	Tafel slope (mV dec^{-1})	Ref.
Ni_3S_2-Ni_2P/NF	130	77.6	This work
CoP/CC	209	129	15
WP/CC	150	102	16
MoP_2/Mo	194	80	17
Ni_3S_2/NF	223	-	18
Ni/NC	219	101	19
Ni/Mo_2C-PC	179	101	20
CoS_2	244	133	21
WN/CC	285	170	22
MoS_2-Ni_3S_2 HNRs/NF	98	61	12
Co-Mo/Ti	75	---	23
Fe-CoP/Ti	78	75	24
C-MoS_2	45	46	25
MoS_2@Ni/CC	91	89	26
$WS_{2(1-x)}Se_{2x}$/$NiSe_2$	88	47	27
MoP_2NS/CC	67	70	28

Table S4. Comparison of overall water splitting performance for the electrolyzer assembled by two Ni_3S_2-Ni_2P/NF electrodes with other reported alkaline electrolyzer assembled by bifunctional catalysts.

Catalysts	Voltage (V) @10 mA cm^{-2}	Electrolytes	Ref.
Ni_3S_2-Ni_2P/NF	1.58	1 M KOH	This work
NiS/Ni foam	1.64	1 M KOH	29
$NiCo_2S_4$ NA/CC	1.68	1 M KOH	30
Ni_3S_2/NF	1.76	1 M KOH	18
Ni-P foam	1.64	1 M KOH	31
$FeNi_3N$/NF	1.62	1 M KOH	32
Ni_2P	1.63	1 M KOH	8
CoSe/Ti	1.65	1 M KOH	33
Ni_5P_4	1.69	1 M KOH	34
Ni_3Se_2/NF	1.61	1 M KOH	35

References

1   K. Fan, H. Chen, Y. Ji, H. Huang, P. M. Claesson, Q. Daniel, B. Philippe, H. Rensmo, F. Li, Y. Luo and L. Sun, *Nat. Commun.*, 2016, **7**, 11981.

2   D. A. Kuznetsov, D. V. Konev, N. y. S. Komarova, A. M. Ionov, R. N. Mozhchil and I. V. Fedyanin, *Chem. Commun.*, 2016, **52**, 9255-9258.

3   F. Song and X. Hu, *Nat. Commun.,* 2014, **5**, 4477.

4   M. Görlin, P. Chernev, J. Ferreira de Araújo, T. Reier, S. Dresp, B. Paul, R. Krähnert, H. Dau and P. Strasser, *J. Am. Chem. Soc.*, 2016, **138**, 5603-5614.

5   C. Dong, X. Yuan, X. Wang, X. Liu, W. Dong, R. Wang, Y. Duan and F. Huang, *J. Mater. Chem. A*, 2016, **4**, 11292-11298.

6   L. A. Stern and X. Hu, *Faraday Discuss.*, 2014, **176**, 363-379.

7   M. Shalom, D. Ressnig, X. Yang, G. Clavel, T. P. Fellinger and M. Antonietti, *J. Mater. Chem. A*, 2015, **3**, 8171-8177.

8   L.-A. Stern, L. Feng, F. Song and X. Hu, *Energy Environ. Sci.*, 2015, **8**, 2347-2351.

9   P. Chen, K. Xu, Z. Fang, Y. Tong, J. Wu, X. Lu, X. Peng, H. Ding, C. Wu and Y. Xie, *Angew. Chem. Int. Ed.*, 2015, **54**, 14710-14714.

10   E. Hu, Y. Feng, J. Nai, D. Zhao, Y. Hu and X. W. Lou, *Energy Environ. Sci.*, 2018, **11**, 872-880.

11   B. Weng, F. Xu, C. Wang, W. Meng, C. R. Grice and Y. Yan, *Energy Environ. Sci.*, 2017, **10**, 121-128.

12   Y. Yang, K. Zhang, H. Lin, X. Li, H. C. Chan, L. Yang and Q. Gao, *ACS Catal.*, 2017, **7**, 2357-2366.

13   P. Li, Z. Jin, J. Yang, Y. Jin and D. Xiao, *Chem. Mater.*, 2015, **28**, 153-161.

14   X. Long, J. Li, S. Xiao, K. Yan, Z. Wang, H. Chen and S. Yang, *Angew. Chem. Int. Ed.*, 2014, **53**, 7584-7588.

15   J. Tian, Q. Liu, A. M. Asiri and X. Sun, *J. Am. Chem. Soc.*, 2014, **136**, 7587-7590.

16   Z. Pu, Q. Liu, A. M. Asiri and X. Sun, *ACS Appl. Mater. Interfaces*, 2014, **6**, 21874-21879.

17   Z. Pu, I. S. Amiinu, X. Liu, M. Wang and S. Mu, *Nanoscale*, 2016, **8**, 17256-17261.

18   L. L. Feng, G. Yu, Y. Wu, G. D. Li, H. Li, Y. Sun, T. Asefa, W. Chen and X. Zou, *J. Am. Chem. Soc.*, 2015, **137**, 14023-14026.

19   X. Zhang, H. Xu, X. Li, Y. Li, T. Yang and Y. Liang, *ACS Catal.*, 2015, **6**, 580-588.

20   Z. Y. Yu, Y. Duan, M. R. Gao, C. C. Lang, Y. R. Zheng and S. H. Yu, *Chem. Sci.*, 2017, **8**, 968-973.

21   H. Zhang, Y. Li, G. Zhang, P. Wan, T. Xu, X. Wu and X. Sun, *Electrochim. Acta*, 2014, **148**, 170-174.

22   J. Shi, Z. Pu, Q. Liu, A. M. Asiri, J. Hu and X. Sun, *Electrochim. Acta*, 2015, **154**, 345-351.

23   J. M. McEnaney, T. L. Soucy, J. M. Hodges, J. F. Callejas, J. S. Mondschein and R. E. Schaak, *J. Mater. Chem. A*, 2016, **4**, 3077-3081.

24   C. Tang, R. Zhang, W. Lu, L. He, X. Jiang, A. M. Asiri and X. Sun, *Adv. Mater.,* 2017, **29**, 1602441.

25   Y. Zang, S. Niu, Y. Wu, X. Zheng, J. Cai, J. Ye, Y. Xie, Y. Liu, J. Zhou, J. Zhu, X. Liu, G. Wang and Y. Qi*an, Nat. Commun.,* 2019, **10**, 1217.

26   Z. Xing, X. Yang, A. M. Asiri and X. Sun, *ACS Appl. Mater. Interfaces,* 2016, **8**, 14521-14526.

27   H. Zhou, F. Yu, J. Sun, H. Zhu, I. K. Mishra, S. Chen and Z. Ren, *Nano lett.*, 2016, **16**, 7604-7609.

28   W. Zhu, C. Tang, D. Liu, J. Wang, A. M. Asiri and X. Sun, *J. Mater. Chem. A*, 2016, **4**, 7169-7173.

29   W. Zhu, X. Yue, W. Zhang, S. Yu, Y. Zhang, J. Wang and J. Wang, *Chem. Commun.*, 2016, **52**, 1486-1489.

30   D. Liu, Q. Lu, Y. Luo, X. Sun and A. M. Asiri, *Nanoscale*, 2015, **7**, 15122-15126.

31   X. Wang, W. Li, D. Xiong and L. Liu, *J. Mater. Chem. A*, 2016, **4**, 5639-5646.

32   B. Zhang, C. Xiao, S. Xie, J. Liang, X. Chen and Y. Tang, *Chem. Mater.*, 2016, **28**, 6934-6941.

33   T. Liu, Q. Liu, A. M. Asiri, Y. Luo and X. Sun, *Chem. Commun.*, 2015, **51**, 16683-16686.

34   M. Ledendecker, S. Krick Calderon, C. Papp, H. P. Steinruck, M. Antonietti and M. Shalom, *Angew. Chem. Int. Ed.*, 2015, **54**, 12361-12365.

35   R. Xu, R. Wu, Y. Shi, J. Zhang and B. Zhang, *Nano Energy*, 2016, **24**, 103-110.